Longitudinal and transverse spin response of ^{12}C in the Δ resonance region

B. Körfgen and F. Osterfeld
Institut für Kernphysik, Forschungszentrum Jülich GmbH, 52425 Jülich, Germany

T. Udagawa
Department of Physics, University of Texas, Austin, Texas 78712
(Received 14 April 1994)

The Δ excitations in nuclei induced by pion and photon scattering are analyzed within the isobar-hole model. The results are compared to those of intermediate energy charge exchange reactions. The similarities and differences between the various probes due to their kinematics and spin-structure are discussed. It is shown that the experimental cross sections for pion and photon induced reactions as well as for the inclusive charge exchange reactions can be consistently described within the isobar-hole model. Of special interest is the coherent pion decay of the Δ resonance which is studied by means of the exclusive reaction ^{12}C(^{3}He, $t\pi^+$)^{12}C (g.s.), by elastic pion scattering, and by pion photoproduction. It turns out that the coherent pion decay of the ^{12}C(^{3}He, $t\pi^+$)^{12}C (g.s.) reaction is intimately related to elastic pion scattering. Most interestingly, both the peak energy and the magnitude of the coherent pion production cross section depend very sensitively on the strength of the Δ-hole residual interaction. The observed energy shift is directly proportional to the nuclear density ρ. This shows that the coherent pions propagate through the nuclear interior. The coherent pion cross section can be used to determine the Landau-Migdal parameter $g'_{\Delta\Delta}$.

PACS number(s): 21.10.Re, 25.20-x, 25.55.Kr, 25.80.Dj

I. INTRODUCTION

Over the past decade, impressive development has taken place in our knowledge of the Δ(1232)-isobar excitation and Δ propagation in nuclei. Much of the progress has been made through both photon- and pion-induced nuclear reactions in the Δ resonance energy region [1,2]. While the nuclear response to photons is found to be practically universal in the Δ region [3–7], i.e., independent of the mass number A, the pion response does show a strong A dependence [8,9]. In particular, the peak position of the pion-nucleus total cross section is systematically shifted downward in energy with mass number A ($\Delta E \approx -15A^{\frac{1}{3}}$ MeV) relative to that of the free πN system [8,9,2]. The different energy dependence of the photon and pion total cross sections can be consistently explained within the isobar-hole model which describes the data in terms of an interplay of the pion, nuclear, and Δ dynamics [1,2,10–12]. In the isobar-hole model one finds that the coherent multiple scattering of the pion in the nucleus leads to a strong energy shift and broadening in the elastic pion-nucleus cross section. The coherent pion propagation combined with the various damping effects produces also a broadening of the Δ resonance in the reaction channels. In photon-induced reactions, however, such a shift is not observed since in this case the coherent multiple scattering of the pion is strongly suppressed [13,14]. Therefore the photon measures only the broadening of the Δ resonance due to the Fermi motion and the nuclear mean field effects. The different information contained in the pion and photon reactions is a result of the different spin structure of the $\pi N\Delta$ and $\gamma N\Delta$ couplings. The $\pi N\Delta$ coupling is purely spin-longitudinal and proportional to $\vec{S}\cdot\vec{q}\,\vec{T}$, while the $\gamma N\Delta$ coupling is purely spin-transverse and proportional to $\vec{S}\times\vec{q}\,\vec{T}$ (where $\vec{S}$ and $\vec{T}$ are the spin and isospin transition operators, respectively, connecting spin-isospin 1/2 and 3/2 states; $\vec{q}$ is the pion or photon momentum, respectively). Both couplings are orthogonal to each other so that in photon-induced reactions the coherent π propagation is greatly inhibited in $\vec{q}$ direction.

Recently, new information on the Δ propagation in nuclei has been obtained from intermediate energy (p,n) and (^{3}He,t) charge exchange reactions [15–17]. Similar to the π-nucleus total cross section data, the inclusive cross section data of the charge exchange reactions show also a substantial downward energy shift of the Δ resonance in nuclei compared to the Δ excitation in the proton target [18–21]. The energy shift amounts to ~70 MeV for nuclei with mass number $A \geq 12$ [18]. Part of this shift (~ 40 MeV) is due to the Fermi motion of the nucleons and the nuclear mean field, but 30 MeV of the shift can only be explained by means of a coherent medium effect on the isovector spin-longitudinal response function [22–26]. In contrast to pion and photon scattering, however, the charge exchange reactions provide a mixed spin-longitudinal (LO)–spin-transverse (TR) probe. Therefore the inclusive charge exchange cross sections consist of two parts of opposite behavior: the LO, or "pionlike" component, which is shifted in energy and the TR, or "photonlike" component, which is not shifted. In Ref. [22], it was shown that the spin-transverse and spin-longitudinal components of the Δ excitation cross section are nearly of the same magnitude. Therefore the energy shift in charge exchange reactions amounts only to 30 MeV instead of the 60 MeV observed in the pion

scattering data.

The aim of the present paper is to show that the data of the various reactions, i.e., the charge exchange reactions and the pion- and photon-induced reactions, can be consistently explained within the isobar-hole model. The difference between the various probes is in their spin-structure and their reaction kinematics. For charge exchange reactions the reaction kinematics is always such that the energy transfer ω is smaller than the three-momentum transfer q ($\omega < q$) while for pion and photon absorption we have the energy-momentum relations $\omega = \sqrt{q^2 + m_\pi^2}$ and $\omega = q$, respectively. From the point of view of the spin-structure, the pion and photon absorption cross sections contain similar information, as the LO and TR components of the inclusive charge exchange cross section. This analogy can even be extended to the exclusive reactions. For example, the coherent pions from the ^{12}C(^{3}He,$t\pi^+$)^{12}C(g.s.) reaction [27–33] show similar features as elastically scattered real pions. We shall show, however, that the coherent pion production reaction is much more useful to display the collective effects in the LO response function than elastic pion scattering itself. Furthermore, although photons excite the nucleus spin-transversely, there is a mixing between the spin-transverse and spin-longitudinal channel due to the finiteness of the nucleus. This mixing is examined by the coherent ^{12}C(γ,π^0)^{12}C(g.s.) reaction. Finally, the spin-transverse response of the nucleus is studied by the Compton scattering which involves a spin-transverse coupling in both the initial and final channels.

In Sec. II we briefly describe the formalism used in the analysis of the pion- and photon-induced reactions. This section is intended as a supplement to the formalism presented in a recent paper [33]. In Sec. III we present the results of our cross section calculations and compare them to the experimental data. We also make various studies of the nuclear medium effect on the Δ with special emphasis to the Δ-hole interaction in the spin-longitudinal channel. Finally, in Sec. IV we give a summary and conclusions.

II. THEORY

In this section we describe the Δ-hole model used in the analysis of the experimental data. The formalism and the methods of calculation were presented already in a recent paper by Udagawa *et al.* [33]. In the present paper we give only those formulas which are connected with pion and photon scattering off nuclei and with pion photoproduction. We refer the reader to Ref. [33] for information on the charge exchange reactions.

A. Elastic pion scattering

We start our formulation by writing down the differential cross section for the elastic pion scattering off a nucleus A. In the reaction a particle-hole (ph) state is created in A. In the present work we restrict the particle p to be a Δ and denote the hole nucleus by B. The differential cross section in the pion-nucleus center-of-mass system (c.m.) is then given by

$$\left(\frac{d\sigma}{d\Omega}\right)_{\rm c.m.} = \frac{1}{(4\pi)^2}\frac{M_A^2}{s}\,|T^\pi|^2, \tag{1}$$

where M_A is the mass of the target and $\sqrt{s}$ is the total energy of the pion-nucleus system. (We use natural units throughout, i.e., $\hbar = c = 1$.) The transition amplitude T^π for elastic pion-nucleus scattering is given as

$$T^\pi(\vec{q}\,'_\pi, \vec{q}_\pi) = \langle \Phi_A \mid F_{\pi N\Delta}(\vec{q}\,'_\pi)\, G\, F^\dagger_{\pi N\Delta}(\vec{q}_\pi) \mid \Phi_A\rangle, \tag{2}$$

where $\mid \Phi_A\rangle$ denotes the target nucleus ground state, $F^\dagger_{\pi N\Delta}(\vec{q}_\pi)$ is the $\pi N\Delta$ excitation operator, and G is the Green's operator propagating the ph state inside the nucleus. The explicit form of G will be discussed in Sec. II B. The $\pi N\Delta$ excitation operator has the form [34,35]

$$F^\dagger_{\pi N\Delta}(\vec{q}_\pi) = \frac{f_{\pi N\Delta}}{M_\pi}\left(\vec{q}_\pi \cdot \vec{S}^\dagger\right) T^\dagger_\nu e^{i\vec{q}_\pi\cdot\vec{r}} \tag{3}$$

where $\vec{S}^\dagger$ and $\vec{T}^\dagger$ are the spin- and isospin-transition operators, respectively. The $\pi N\Delta$ coupling constant is fixed from pion-nucleon scattering data and has the value $f^2_{\pi N\Delta}/4\pi = 0.324$. The index $\nu = \pm 1$ distinguishes between $\pi^\pm$ scattering.

Using the optical theorem the total pion-nucleus cross section can be given by

$$\sigma^\pi_{\rm tot} = \frac{M_A}{\mid \vec{q}_\pi \mid \sqrt{s}}\,{\rm Im}\,[-T^\pi(\vec{q}_\pi, \vec{q}_\pi)], \tag{4}$$

where $\vec{q}_\pi$ is the three-momentum of the pion in the c.m. and $T^\pi(\vec{q}_\pi, \vec{q}_\pi)$ is the transition amplitude at zero degree scattering angle.

B. Propagation of the Δ inside the nucleus

The excitation operator $F^\dagger_{\pi N\Delta}(\vec{q}_\pi)$ of Eq. (3) initially excites the doorway state

$$\mid \rho_\pi\rangle = F^\dagger_{\pi N\Delta}(\vec{q}_\pi) \mid \Phi_A\rangle, \tag{5}$$

which is then propagated by the many-body Green's operator G, resulting in the wave function [33]

$$\mid \psi\rangle = G \mid \rho_\pi\rangle = \frac{1}{\omega + i\Gamma_\Delta/2 - H_B - T_\Delta - U_\Delta - V_{\Delta N,\Delta N}} \mid \rho_\pi\rangle. \tag{6}$$

The wave function $|\psi\rangle$ describes the intermediate $(B+\Delta)$ system. H_B is the Hamiltonian of nucleus B, $\Gamma_\Delta(\omega)$ is the energy dependent free decay width of the Δ, T_Δ, and U_Δ are the kinetic energy operator and the Δ-nucleus one-body potential, respectively, and $V_{\Delta N,\Delta N}$ is the ΔN^{-1} residual interaction. For the target ground state wave function a pure shell model configuration was assumed. The single particle wave functions were generated from a Woods-Saxon potential with the geometrical parameters $a_0 = a_{so}$=0.53 fm, and $r_0 = r_{so} = r_C$=1.20 fm and the spin-orbit strength V_{so} =5.53 MeV. The strength parameters for the proton and neutron potentials were fixed as V_p=65.7 MeV and V_n=66.0 MeV, respectively. The Δ-nucleus potential is taken as a complex Woods-Saxon potential, $U_\Delta = V_\Delta + iW_\Delta$, with radius parameter $R = 1.1A^{1/3}$ fm and diffuseness $a = 0.53$ fm. The depths for the real and imaginary potential are $V_\Delta = -35$ MeV and $W_\Delta = -40$ MeV, respectively [12]. Note that V_Δ is assumed to be the sum of the Δ-nucleus single particle potential (depth=$-$65 MeV) and of the real part of the Δ spreading potential (strength=+30 MeV). W_Δ represents the imaginary part of the spreading potential. The spreading potential accounts in a phenomenological way for the Pauli-blocking effects [1,2] and the increase of the Δ width in nuclei due to decay channels such as $\Delta N \to NN$.

The residual interaction, $V_{\Delta N,\Delta N}$, is treated within the $\pi + \rho + g'_{\Delta\Delta}$ model (see [17] for all references). In the ρ exchange we keep only the tensor interaction and drop the central part, assuming that the latter can be effectively included in the short-range interaction [22,33]. In the momentum representation, $V_{\Delta N,\Delta N}$ may be given as a sum of LO and TR components

$$V_{\Delta N,\Delta N} = [V^L_{\Delta N,\Delta N}(\vec{S}_2\cdot\hat{q})(\vec{S}_1^\dagger\cdot\hat{q}) + V^T_{\Delta N,\Delta N}(\vec{S}_2\times\hat{q})\cdot(\vec{S}_1^\dagger\times\hat{q})]\,(\vec{T}_2\cdot\vec{T}_1^\dagger), \quad (7)$$

where

$$V^L_{\Delta N,\Delta N}(\omega,q) = \hbar c\frac{f_\pi^2(t)}{m_\pi^2}\left[g'_{\Delta\Delta} + \frac{q^2}{\omega^2-q^2-m_\pi^2+i\varepsilon} - \frac{2}{3}\frac{m_\pi^2}{f_\pi^2(t)}\frac{f_\rho^2(t)}{m_\rho^2}\frac{q^2}{\omega^2-q^2-m_\rho^2+i\varepsilon}\right],$$

$$V^T_{\Delta N,\Delta N}(\omega,q) = \hbar c\frac{f_\pi^2(t)}{m_\pi^2}\left[g'_{\Delta\Delta} + \frac{1}{3}\frac{m_\pi^2}{f_\pi^2(t)}\frac{f_\rho^2(t)}{m_\rho^2}\frac{q^2}{\omega^2-q^2-m_\rho^2+i\varepsilon}\right]. \quad (8)$$

In Eq. (8), the $f_i(t=\omega^2-\vec{q}^{\,2})$ are the meson-baryon vertex form factors which we assume to be $f_i(t) = f_{iN\Delta}\,(\Lambda_i^2 - m_i^2)/(\Lambda_i^2 - t)$ $(i = \pi,\ \rho)$, and m_i and Λ_i are the mass and cutoff mass of the meson i, respectively. The various parameters are fixed as follows: $f^2_{\pi N\Delta}/4\pi = 0.324$, $f^2_{\rho N\Delta}/4\pi = 16.63$, $m_\pi = 0.14$ GeV, $m_\rho = 0.77$ GeV, $\Lambda_\pi = 1.20$ GeV, and $\Lambda_\rho = 2$ GeV. The Landau-Migdal parameter $g'_{\Delta\Delta}$ describes the short-range correlations for $\Delta N^{-1} \to \Delta N^{-1}$ transitions. In the present calculations, we use the minimal $g'_{\Delta\Delta}$ that cancels out the δ-function-like piece of the π-exchange potential. Then the Landau-Migdal parameter $g'_{\Delta\Delta} \approx 0.33$ (in units of $J_{\pi\Delta\Delta} = \hbar c f^2_{\pi N\Delta}/m_\pi^2 \approx 1600$ MeV fm^3). Note that this parameter depends on the choice of U_Δ. A discussion of the interrelation between U_Δ and $g'_{\Delta\Delta}$ is given in Refs. [36,37] where the authors use a microscopic model for the Pauli blocking and Δ spreading effects. In our approach we treat U_Δ and $g'_{\Delta\Delta}$ on a phenomenological level. These values are finally fixed from the requirement to reproduce the peak position of the Δ resonance in the various reactions. This will be shown in more detail in Sec. III.

Inserting Eq. (5) in Eq. (2) one can rewrite the transition amplitude for elastic pion scattering in the following way:

$$T^\pi = \langle\rho'_\pi \mid G \mid \rho_\pi\rangle, \quad (9)$$

where we have introduced the state $\langle\rho'_\pi \mid$ which describes the deexcitation process of the $(B+\Delta)$ system into the ground state of A and an outgoing pion with momentum $\vec{q}'_\pi$. The explicit formulas for the source function $|\rho_\pi\rangle$ and the transition amplitude T^π are derived in appendixes A and B, respectively. For 0° scattering the ingoing and outgoing pion momenta are identical. Therefore the total pion-nucleus cross section can be written as

$$\sigma^\pi_{\rm tot} = \frac{M_A}{|\vec{q}_\pi|\sqrt{s}}\,{\rm Im}\,[-\langle\rho_\pi \mid G \mid \rho_\pi\rangle]\,. \quad (10)$$

C. Coherent pion photoproduction

In order to calculate the transition amplitude for coherent pion photoproduction we only have to replace the $\pi N\Delta$ excitation operator in (2) by the corresponding $\gamma N\Delta$ excitation operator [38]; the transition amplitude is then given by

$$T^{\gamma\pi} = \langle\Phi_A \mid F_{\pi N\Delta}(\vec{q}'_\pi)\,G\,F^\dagger_{\gamma N\Delta}(\vec{q}_\gamma) \mid \Phi_A\rangle = \langle\rho'_\pi \mid G \mid \rho_\gamma\rangle, \quad (11)$$

where $|\rho_\gamma\rangle$ is the doorway state excited by the incident photon. The explicit formula for this doorway state is given in Appendix A. The $\gamma N\Delta$ excitation operator is known to have the following form [34,35]:

$$F^\dagger_{\gamma N\Delta}(\vec{q}_\gamma) = \frac{f_{\gamma N\Delta}}{M_\Delta}\left(\hat{\varepsilon}_{\vec{q}\lambda}\times\vec{q}_\gamma\right)\cdot\vec{S}^\dagger\ T_0^\dagger e^{i\vec{q}_\pi\cdot\vec{r}}, \quad (12)$$

where $\hat{\varepsilon}_{\vec{q}\lambda}$ is the polarization vector of the photon with momentum $\vec{q}_\gamma$ and helicity λ; the $\gamma N\Delta$ coupling constant is $f_{\gamma N\Delta} = 1.03$ [13]. The differential cross section for coherent pion photoproduction in the c.m. system is then given by

$$\left(\frac{d\sigma}{d\Omega}\right)_{\rm c.m.} = \frac{1}{(4\pi)^2}\frac{M_A^2}{s}\frac{|\vec{q}'_\pi|}{|\vec{q}_\gamma|}\frac{1}{2}\sum_\lambda |T^{\gamma\pi}|^2\,. \quad (13)$$

Here E_γ and $\vec{q}_\gamma$ (E'_π and $\vec{q}'_\pi$) are the ingoing photon (outgoing pion) energy and momentum in the c.m. system, respectively.

D. Elastic Compton scattering

The transition amplitude for elastic Compton scattering exciting the Δ resonance can be obtained from Eq. (2) by replacing $F_{\pi N\Delta}$ through $F_{\gamma N\Delta}$, resulting in

$$T^{\gamma}_{\Delta} = \langle \Phi_A \mid F_{\gamma N\Delta}(\vec{q}'_{\gamma})\, G\, F^{\dagger}_{\gamma N\Delta}(\vec{q}_{\gamma}) \mid \Phi_A \rangle = \langle \rho'_{\gamma} \mid G \mid \rho_{\gamma} \rangle . \quad (14)$$

From studies of the Compton scattering off the nucleon it is known that the resonant process via an intermediate Δ alone is not sufficient to reproduce the experimental data [13]. There is a nonresonant contribution to s-wave charged pion photoproduction which we describe by using the Kroll-Ruderman (KR) ansatz [39,40]. This background process corresponds to the excitation of an intermediate π-nucleon system with total angular momentum $J = \frac{1}{2}$. The T matrix for Compton scattering on ^{12}C via an intermediate π-nucleon system with $J = \frac{1}{2}$ is then given by

$$T^{\gamma}_{\rm KR} = \langle \Phi_A \mid F^{*}_{\rm KR}(\vec{q}', \lambda') G_{\rm KR} F_{\rm KR}(\vec{q}, \lambda) \mid \Phi_A \rangle \quad (15)$$

where

$$F_{\rm KR}(\vec{q}, \lambda) = \sqrt{2\alpha}(4\pi)\frac{f_{\pi NN}}{m_{\pi}} h(E)(\hat{\varepsilon}_{\vec{q}\lambda} \cdot \vec{\sigma}) e^{i\vec{q}\cdot\vec{r}}. \quad (16)$$

describes the s-wave charged pion photoproduction operator and $h(E)$ introduces a phenomenological energy dependence fixed in Compton scattering on the nucleon [13]. The propagator $G_{\rm KR}$ of the intermediate π-nucleus system is approximated by a δ function with a strength factor calculated from the π-nucleon system [13]

$$G_{\rm KR}(E, \vec{r}', \vec{r} \approx \delta^3(\vec{r}' - \vec{r}) \int \frac{d^3k'}{(2\pi)^3} \frac{1}{2\omega_{k'}} \frac{m_N}{\varepsilon_{k'}} \left| \frac{v(k')}{v(k)} \right|^2 \times \frac{1}{E - (\omega_{k'} + \varepsilon_{k'}) + i\varepsilon}. \quad (17)$$

Here E is the total energy of the π-nucleon system, k' is its c.m. momentum, and $v(k) = (1 + k^2/\beta^2)^{-1}$ is the pion-nucleon form factor with $\beta = 300$ MeV/c [13].

The differential cross section for Compton scattering is then given by the sum of resonance and background terms as

$$\left(\frac{d\sigma}{d\Omega}\right)_{\rm c.m.} = \frac{1}{(4\pi)^2} \frac{M_A^2}{s} \frac{1}{2} \sum_{\lambda\lambda'} |T^{\gamma}_{\Delta} + T^{\gamma}_{\rm KR}|^2 . \quad (18)$$

The explicit formula for the transition amplitude is given in Appendix C. Analogous to Eq. (10), the total photon-nucleus cross section is given by the sum of resonant and nonresonant contributions as

$$\sigma^{\gamma}_{\rm tot} = \frac{M_A}{|\vec{q}_{\gamma}| \sqrt{s}} \, {\rm Im}\left[-\langle \rho_{\gamma} \mid G \mid \rho_{\gamma} \rangle - T^{\gamma}_{\rm KR} \right] . \quad (19)$$

III. RESULTS AND DISCUSSION

In this section we present our results for pion and photon scattering off nuclei in the Δ resonance region. Special emphasis is placed on the difference between the LO and TR excitation and deexcitation of the nucleus and the LO-TR (TR-LO) interference. We compare the results of real pion and photon scattering with those of the charge exchange reactions.

A. Pion and photon total cross sections

In Figs. 1(a) and (b) we first analyze total cross section data for pion- [8,9] and photon-scattering [6] off ^{12}C in the Δ resonance region. The dash-dot curves represent the sum of the free pion-nucleon cross sections ($A \times \bar{\sigma}_{\pi N}$) and free photon-nucleon cross sections ($A \times \bar{\sigma}_{\gamma N}$), respectively, where A is the mass number and $\bar{\sigma} = 1/2(\sigma_p + \sigma_n)$. In case of pion scattering, a dramatic reduction and broadening in the cross section is observed between the free Δ resonance and the Δ in the nucleus. Such a broadening and reduction does not occur for photon scattering. The reason for this is well known [2,11] and is mainly due to the multiple scattering of the pion in the nucleus. The $V_{\Delta N,\Delta N}$ couples strongly to the pion (LO) channel, but only weakly to the photon (TR) channel. As a consequence, the pion scattering takes place primarily at the nuclear surface while the photon penetrates the nuclear volume. The correctness of this picture can be proven by a comparison of calculations with and without inclusion of the residual interaction $V_{\Delta N,\Delta N}$. The

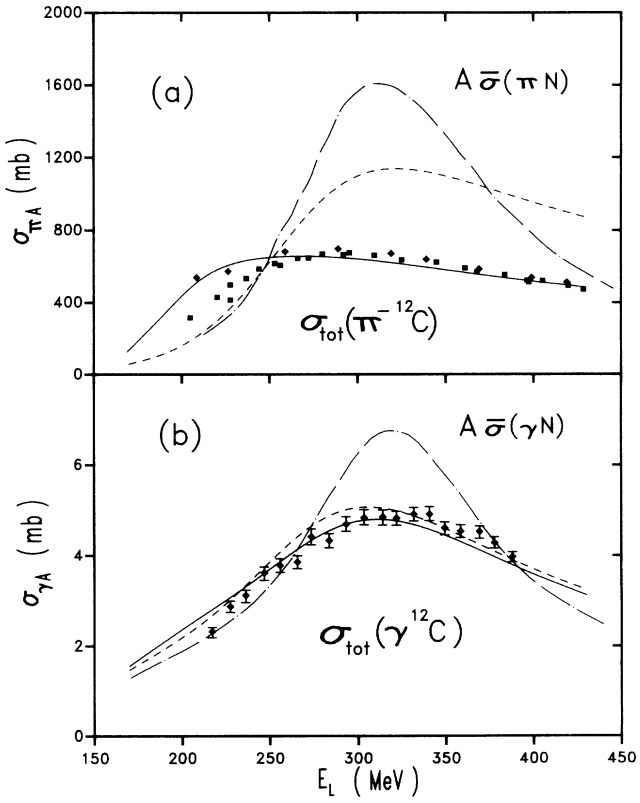

FIG. 1. The pion- and photon-nucleus total cross sections for ^{12}C. The photon data are taken from Ref. [6] and the pion data are taken from Refs. [8] (squares) and [9] (circles). The dash-dot curve in (a) represents the incoherent sum of pion-nucleon total cross sections ($A \times \bar{\sigma}_{\pi N}$), and the dash-dotted curve in (b) represents the incoherent sum of total photon-nucleon cross sections ($A \times \bar{\sigma}_{\gamma N}$). The solid and dashed curves represent calculations for the total cross sections with and without inclusion of the residual interaction, respectively.

results are shown in Fig. 1 by the solid ($V_{\Delta N,\Delta N} \neq 0$) and dashed ($V_{\Delta N,\Delta N} = 0$) curves, respectively. Because of $V_{\Delta N,\Delta N} = 0$, the dashed curves contain only effects of the nuclear mean field and the Fermi motion. By comparing these curves to the free cross sections, one observes that for both pion and photon scattering the calculated nuclear cross sections are reduced by a factor of ~1.4 and broadened by the Fermi motion in a similar way. The inclusion of the residual interaction reduces the pion cross section further, but leaves the photon cross section essentially unchanged. In addition, the pion cross section is shifted down in energy due to the attractiveness of the pion-exchange interaction. The small effect of $V_{\Delta N,\Delta N}$ on the shape and magnitude of the total photon nucleus cross section shows that this observable can be used to determine the parameters of the Δ mean field. Therefore the good description of the data by our calculations indicates that we treat the Δ mean field correctly. Similarly, the large effect of $V_{\Delta N,\Delta N}$ on the pion cross section gives constraints on the strength of the residual interaction in the LO channel.

B. Elastic pion scattering

Because of the strong pion-nucleon interaction in the resonance region, the mean free path of the pion in the nuclear medium reduces to less than 1 fm. This has immediate consequences for the differential cross sections which look like diffraction from a black disc. In Figs. 2 and 3 we show the differential cross sections for six different incident pion energies covering the whole Δ resonance energy region. The solid and dashed curves are calculated with and without inclusion of $V_{\Delta N,\Delta N}$. One can recognize that the residual interaction is very important to reproduce the experimental data. In particular, it reduces the cross section at forward angles by a factor of $\sim$ 4 relative to the results with $V_{\Delta N,\Delta N} = 0$ and gives the right position of the minima and maxima of the diffraction pattern.

In Fig. 4 we compare both the calculated integrated elastic cross section and the calculated reaction cross section ($\sigma_r = \sigma_{\rm tot} - \sigma_{\rm el}$) with data [9]. The cross sections are plotted as function of the incident pion kinetic energy. One can see that both the elastic and the reaction cross sections are described well by our calculations. The broadening and shift of the elastic cross section towards

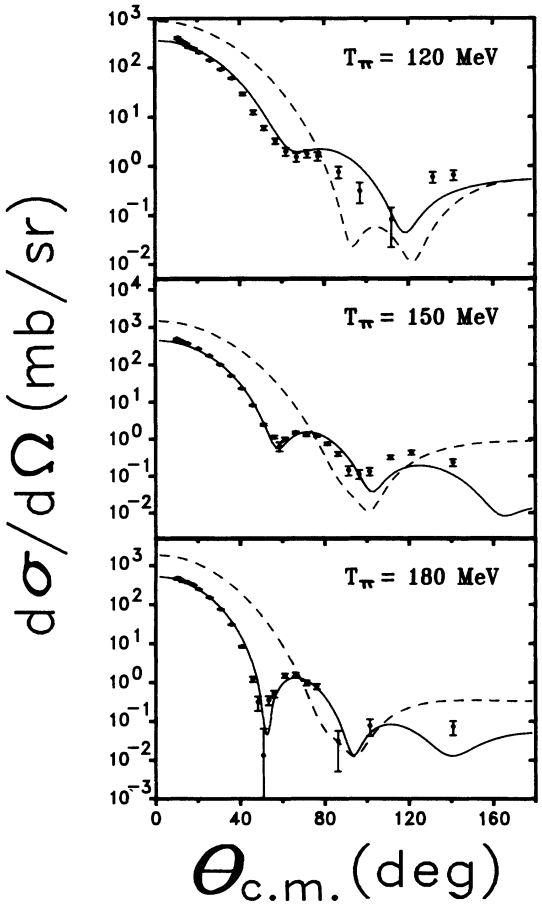

FIG. 2. Differential cross sections for elastic π^- scattering off ^{12}C at incident pion kinetic energies of T_π = 120 MeV, T_π = 150 MeV, and T_π = 180 MeV [9]. The solid and dashed curves show the results with and without inclusion of the residual interaction, respectively.

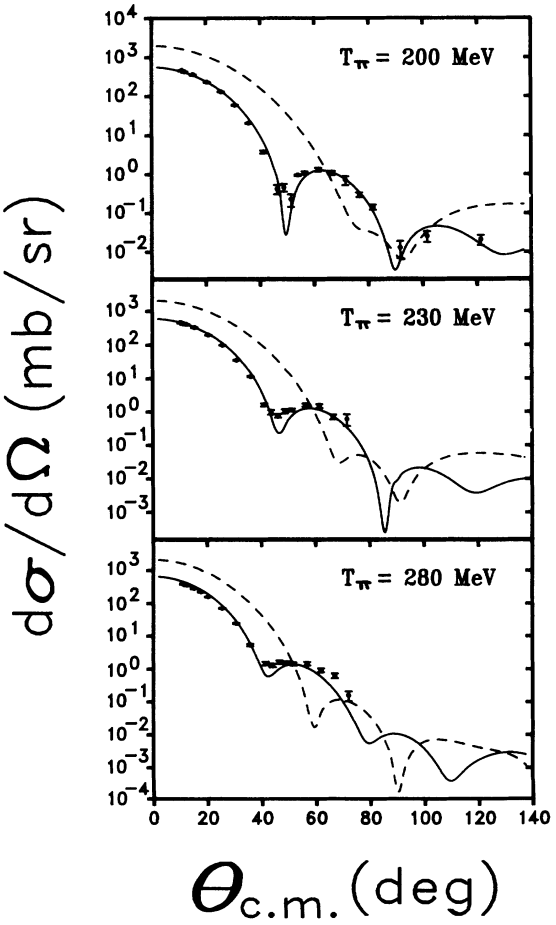

FIG. 3. Same as in Fig. 2, but now for T_π = 200 MeV, T_π = 230 MeV, and T_π = 280 MeV.

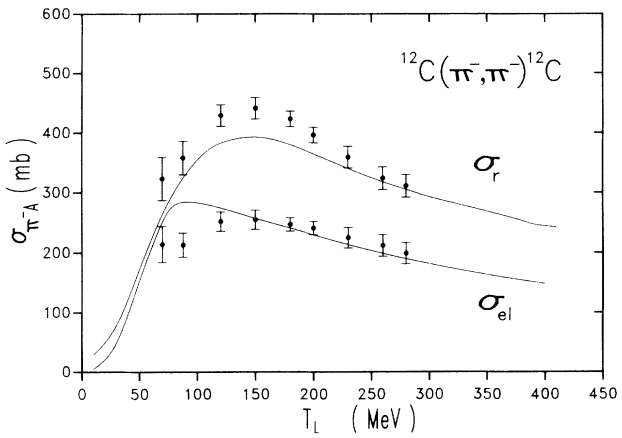

FIG. 4. Integrated elastic and reaction cross sections for pion scattering off ^{12}C. The curves represent Δ-hole calculations. The data are taken from Ref. [9].

lower pion kinetic energies is an effect of the attractive pion-exchange interaction in the nucleus. This multiple scattering process of the pion in the nucleus leads to the strong coupling to the reactions channels and hence to the large reaction cross section which is the dominant part of the total cross section.

C. Coherent pion photoproduction

The coherent pion photoproduction $^{12}C(\gamma,\pi^0)^{12}C(g.s.)$ measures the mixing between the spin-transverse and spin-longitudinal channels. In an infinite system, like nuclear matter, these channels are completely decoupled but in a finite nucleus they are coupled due to the surface effects. The spin-structure of the excitation $(\vec{S}^\dagger \times \vec{q}_\gamma)$ and deexcitation $(\vec{S} \cdot \vec{q}'_\pi)$ operators in coherent pion photoproduction makes the angular distributions proportional to $\mid \vec{q}_\gamma \times \vec{q}'_\pi \mid = q_\gamma q'_\pi \sin\theta_\pi$ which vanishes for $\theta_\pi = 0°$ and peaks at $\theta_\pi = 90°$. However, an additional momentum transfer dependent factor comes from the overlap integral of Eq. (11) which shifts the peak position of the angular distribution to smaller angles. In Fig. 5 we compare the calculated differential pion photoproduction cross section at two different incident photon momenta with the data. The solid and dashed curves represent calculations with and without inclusion of the residual interaction $V_{\Delta N,\Delta N}$. One can recognize that the calculation at incident photon momentum $k_\gamma^L = 235$ MeV/c [Fig. 5(a)] describes the experimental angular distributions rather well. In Fig. 5(b) ($k_\gamma^L = 291$ MeV/c) the calculation with inclusion of $V_{\Delta N,\Delta N}$, however, underestimates the absolute magnitude of the cross section. The reason for this underestimate is mainly the experimental energy resolution which amounts only to $\sim$ 15 MeV. Therefore the experimental data include, in addition to the coherent pions, pions from other reaction processes where the final nucleus is left in an excited state. The comparison of the dashed and solid curves shows that there is an effect of the mul-

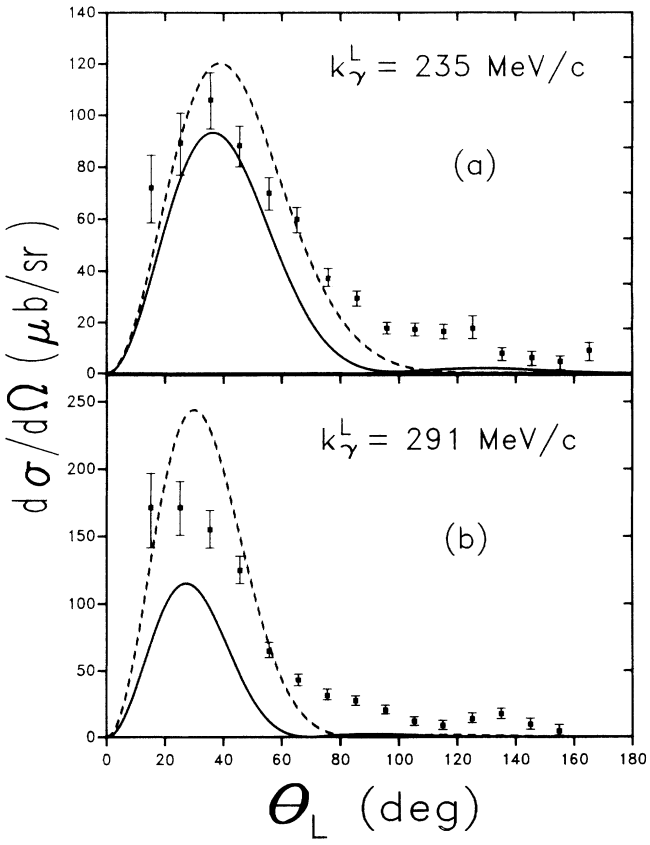

FIG. 5. Differential cross sections for coherent pion photoproduction at incident photon momenta of (a) $k_\gamma^L = 235$ MeV/c and (b) $k_\gamma^L = 291$ MeV/c in comparison with the data [5]. The solid and dashed curves show cross sections with and without inclusion of the residual interaction, respectively.

tiple pion scattering in the nucleus increasing with the in-going photon momentum. This can be seen even more clearly in Fig. 6, where we compare the calculated spectra for the $^{12}C(\gamma,\pi^0)^{12}C(g.s.)$ reaction with the data. One can note that the calculations with and without inclusion of $V_{\Delta N,\Delta N}$ differ in magnitude and shape. The

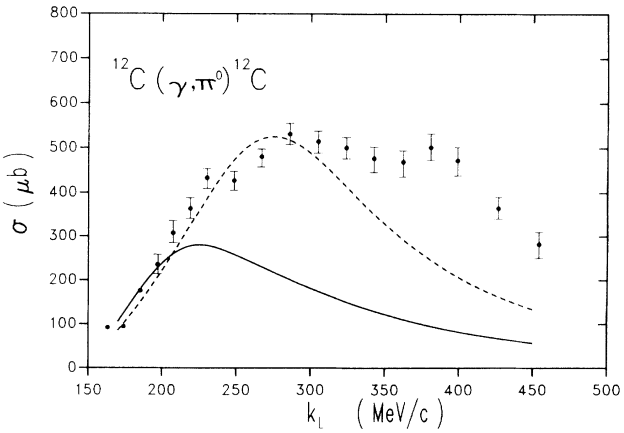

FIG. 6. Integrated cross sections for coherent pion photoproduction on ^{12}C. The data are taken from Arends *et al.* [5]. The solid and dashed curves represent cross section calculations with and without inclusion of $V_{N\Delta,N\Delta}$, respectively.

reduction in the calculation, including the residual interaction (solid curve) relative to that without $V_{\Delta N,\Delta N}$ (dashed curve) and the shift of the peak position of the solid curve by $\sim$ 80 MeV relative to the dashed curve, is an effect of the attractive residual interaction in the spin-longitudinal channel.

New data for coherent pion photoproduction at outgoing pion angle $\theta_\pi^L = 60°$ have been taken at MAMI B in Mainz. These preliminary data [41] seem to indicate that the data in Fig. 6 [5] are dominated by inelastic pions for photon momenta above $k_\gamma^L = 250$ MeV/c. The new experiment done with the spectrometer CATS allows one to distinguish between coherent and inelastic pions due to the very good energy resolution of the CATS detector.

D. Real versus "virtual" pion scattering

In the charge exchange reactions the target is exposed to the virtual pion- and ρ-meson fields produced by the projectile-ejectile system. The pionlike interaction excites the LO response function of the target while the ρ-meson-like interaction excites the TR response function. Due to the kinematics the virtual meson fields obey the energy-momentum relation $\omega < q$ and thus explore the LO and TR response functions in an $(\omega, \vec{q})$ region which is inaccessible to real pion and photon scattering. From the analysis of the ^{12}C(^{3}He, t) reaction at $E = 2$ GeV we know [22] that the LO and TR response functions are excited with roughly equal strength. The two responses can be experimentally separated by measuring the exclusive ^{12}C(^{3}He, $t\pi^+$)^{12}C(g.s.) reaction. This reaction triggers selectively on the LO channel. In Fig. 7(a) we show the measured data of Hennino *et al.* [28] and compare them to previously [33] calculated angular distributions. The dashed curve is the result from both LO and TR excitation while the solid curve is the result of LO excitation alone. The small difference between both curves shows the dominance of the LO over the TR excitation in this reaction. The TR excitation is suppressed because of the unfavorable TR-LO channel mixing. The shape of the angular distribution is strongly forward peaked. This is an effect of the spin-structure of the excitation $(\vec{S}^\dagger \cdot \vec{q})$ and deexcitation $(\vec{S} \cdot \vec{q}'_\pi)$ operators involved in the LO channel. The product of both operators is proportional to $qq'_\pi \cos\theta_\pi$ and peaks at $\theta_\pi = 0°$. In Fig. 7(b) we show the corresponding elastic pion cross section at an appropriately chosen incident energy. One observes the direct proportionality between the coherent pion production cross section of Fig. 7(a) and the elastic pion cross section of Fig. 7(b). We remark that the coherent pion production process in the ^{12}C(^{3}He, $t\pi^+$)^{12}C(g.s.) reaction can be viewed as "virtual" pion scattering off ^{12}C, where the initially off-mass shell pion is converted into an on-mass shell pion when the pion is emitted from the nucleus. The momentum needed to lift the pion on its mass shell is provided by the recoil nucleus.

In Fig. 8 we show angular distributions for the spin-transversely excited coherent pion production in charge exchange reactions [Fig. 8(a)] and for the pion photoproduction [Fig. 8(b)]. Because of the $(\vec{S}^\dagger \times \vec{q})$ structure of the excitation operators, the calculated angular distributions (solid curves) are now proportional to $(qq'_\pi)^2 \sin^2\theta_\pi$ and vanish at $\theta_\pi = 0°$. This property is directly confirmed by the pion photoproduction data [5]. It can be noted that the calculated TR angular distribution in Fig. 8(a) peaks at a slightly smaller angle than the angular distribution of the pion photoproduction in Fig. 8(b). The reason for this is twofold: on the one hand the charge exchange reaction involves a larger momentum transfer than the pion photoproduction. Therefore the nuclear form factor suppresses the cross section at higher pion angles in the charge exchange reaction. On the other hand the (^{3}He,t) form factor also cuts off the cross section at high momentum transfers, whereas the $\gamma N\Delta$ coupling for real photon scattering has no such form factor.

In Fig. 9 we compare the calculated ^{12}C(^{3}He, $t\pi^+$)^{12}C(g.s.) coincidence cross section with the measured data of Hennino *et al.* [28]. The solid and the dashed curve represent calculations with Landau-Migdal parameters of $g'_{\Delta\Delta} = 0.33$ and $g'_{\Delta\Delta} = 0.4$, respectively. We find that both the magnitude and the peak position of the cal-

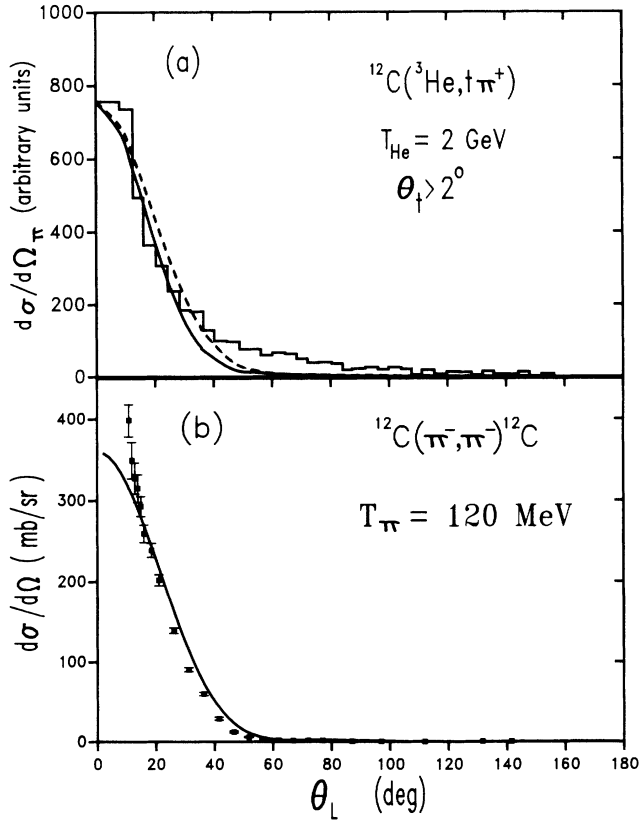

FIG. 7. Angular distributions of coherent pions for (a) the ^{12}C(^{3}He,$t\pi^+$)^{12}C(g.s.) reaction at $T_{He} = 2$ GeV and for (b) the elastic pion scattering off ^{12}C at $T_\pi = 120$ MeV. (a) The dashed curve represents the result of the complete calculation. The solid curve shows the contribution to the pion production cross section resulting from the LO excitation of the nucleus. The data are taken from Ref. [28]. (b) The solid curve represents the calculated elastic pion cross section. The data are taken from Ref. [9].

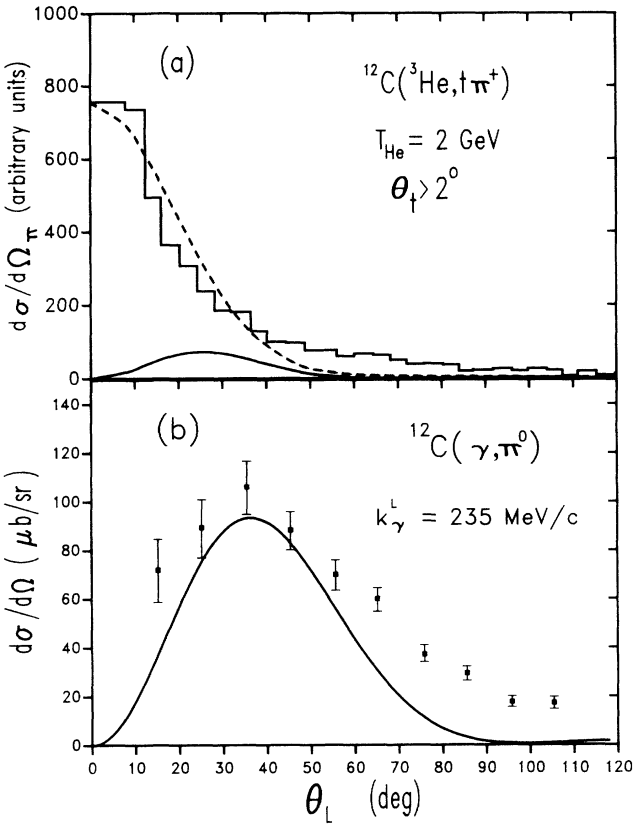

FIG. 8. Angular distributions of coherent pions for (a) the ^{12}C(^{3}He,$t\pi^+$)^{12}C(g.s.) at T_{He} = 2 GeV and for (b) the coherent pion photoproduction on ^{12}C. (a) The dashed curve represents the result of the complete calculation. The solid curve represents the contribution to the pion production cross section resulting from the TR excitation of the nucleus. (b) The data for coherent pion photoproduction are taken from Ref. [5]. The solid curve represents the result of our calculation.

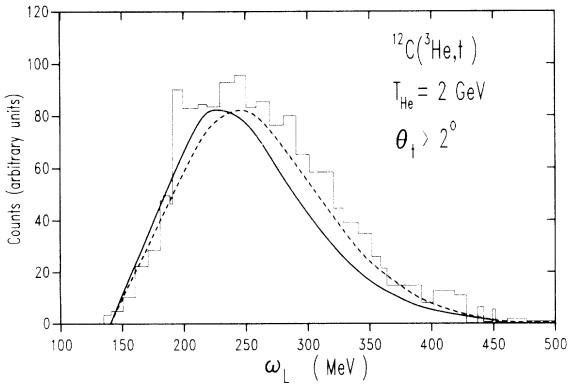

FIG. 9. Pion coincidence spectrum for the ^{12}C(^{3}He,t) reaction at T_{He} = 2 GeV and triton scattering angle $\theta_t \geq 2°$. The data are taken from [28]. The solid and dashed curves represent cross section calculations with Landau-Migdal parameters of $g'_{\Delta\Delta}$ = 0.33 and $g'_{\Delta\Delta}$ = 0.4, respectively. The dashed curve has been multiplied with a factor of 1.5 in order to compare the peak positions.

culated cross section are very sensitive to the choice of the $g'_{\Delta\Delta}$ parameter. While the solid curve reproduces the magnitude of the measured coherent pion production cross section very well [33] the dashed curve was multiplied by a factor of $\sim$ 1.5 to match the data. The energy shift ΔE between both curves is directly proportional to the change in $g'_{\Delta\Delta}$, namely $\Delta E \approx \Delta g'_{\Delta,\Delta}(\hbar c f^2_{\pi N\Delta}/m^2_\pi)\rho_0$ with ρ_0 = 0.17 fm^{-3} being the central nuclear density. The proportionality of ΔE to ρ_0 is due to the fact that the coherent pions come from the nuclear interior. The (^{3}He,t) kinematics force the pions to travel into the direction of the momentum transfer $\vec{q}$. Therefore most of the coherent pions are detected in this direction. By changing the triton emission angle and the triton energy loss one can vary $\vec{q}$ and ω and can map out the energy and momentum dependence of the ΔN^{-1} residual interaction.

Although elastic pion scattering is sensitive to the residual interaction, we do not find such a linear dependence of the energy shift on $V_{\Delta N,\Delta N}$, as we find in case of the ^{12}C(^{3}He,$t\pi^+$)^{12}C(g.s.) reaction. The reason for this is that the pion elastic scattering and the (^{3}He,t) reaction probe the LO nuclear reponse function in different kinematic regions. The pion explores the response along the kinematic line $\omega = \sqrt{q^2 + m^2_\pi}$ while the (^{3}He,t) reaction explores the region $\omega < q$. From theoretical studies of the LO response function in the Δ resonance region [16,24] we know that due to the attractive pion exchange interaction the LO response receives its maximum strength (peak position) near ω = 210 MeV and q = 230 MeV/c [16,24]. This kinematic region is inaccessible to pions, but is accessible to the (^{3}He,t) reaction. Therefore the coherent pion spectrum of the ^{12}C(^{3}He,$t\pi^+$)^{12}C(g.s.) reaction provides an (ω, q) cut through the peak of the LO response function. The shape of the coherent pion pro-

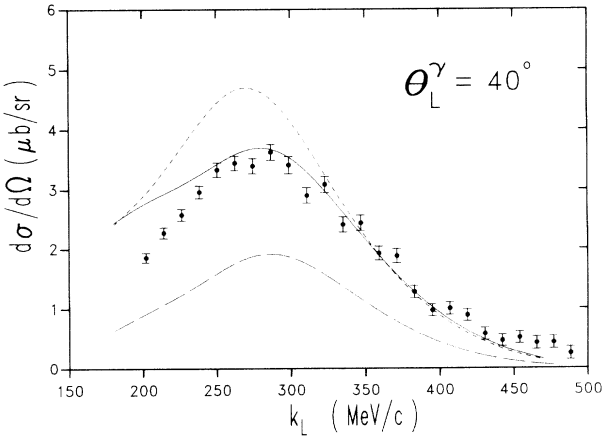

FIG. 10. Differential cross sections for elastic Compton scattering off ^{12}C as function of the incoming photon momentum at a fixed photon angle of θ_γ^L = 40°. The long dashed curve shows the result with intermediate Δ excitation alone. The solid and short-dashed curves represent the results with and without inclusion of the residual interaction, respectively. The latter calculations include the Kroll-Ruderman background contribution, as described in the text. The data are taken from Wissmann [42].

duction spectrum in Fig. 9 directly reflects the shape of the LO strength function along the kinematic cut determined by the (^{3}He,t) reaction.

E. Elastic Compton scattering

Compton scattering corresponds to TR excitation and deexcitation of the nucleus and shows in how far effects of the pion are still visible in the TR-TR channel. In Fig. 10 we show the differential cross section for elastic Compton scattering off ^{12}C at an outgoing photon angle of $\theta_\gamma^L = 40°$ [42]. The long-dashed curve shows the result of our calculation with an intermediate Δ alone (14). In the calculation of the short-dashed and solid curve we included beside the Δ a background contribution (15). The solid and short-dashed curves represent our results with and without inclusion of the residual interaction, respectively. Even in Compton scattering, i.e., spin-transverse excitation and spin-transverse deexcitation, there is an effect of the multiple scattering in the medium. Including the residual interaction, we get a good description of the data at photon energies higher than 250 MeV. At lower energies where the background becomes more important there is a discrepancy between the data and our calculation.

IV. SUMMARY AND CONCLUSIONS

We have studied the spin-isospin response of nuclei in the Δ resonance region by means of real pion and photon scattering and by means of intermediate energy charge exchange reactions. We have shown that the inclusive and exclusive data of the various reactions can be consistently explained within the isobar-hole model. The difference between the various probes is in their spin-structure and their reaction kinematics. We find that the TR response is mainly sensitive to the parameters of the Δ mean field while the LO response is very sensitive to the Δ-hole residual interaction. Our choice of the Δ-hole residual interaction can consistently describe data of pion and photon scattering, pion photoproduction, and coherent pion production in exclusive charge exchange reactions. We have shown that the coherent pion production reaction, i.e., the ^{12}C(^{3}He,$t\pi^+$)^{12}C(g.s.) reaction, is very useful to display the collective effects in the LO response function. Most interestingly, both the peak energy and the magnitude of the coherent pion cross section depend very sensitively on the strength of the Δ-hole residual interaction. The observed energy shift is directly proportional to the nuclear density ρ. This shows that the coherent pions experience multiple scattering and propagate through the nuclear interior. The energy shift observed in the ^{12}C(^{3}He,$t\pi^+$)^{12}C(g.s.) reaction can be used to determine the Landau-Migdal parameter $g'_{\Delta\Delta}$. We find a value of $g'_{\Delta\Delta} \sim 0.333$ in units of 1600 MeV fm^3.

ACKNOWLEDGMENTS

The authors acknowledge many useful discussions with P. Oltmanns. One of us (T.U.) wants to thank Professor J. Speth for the warm hospitality extended to him during various visits of the Forschungszentrum Jülich. This work was supported in part by the Graduiertenkolleg "Die Erforschung subnuklearer Strukturen der Materie" at the University of Bonn and by the U.S. Department of Energy under Contract No. DE-FG05-84-ER40145.

APPENDIX A: EXPLICIT FORMULAS FOR THE PION- AND PHOTON-SOURCE FUNCTIONS

In this appendix, we derive the formulas of the radial source functions for pion and photon scattering. In order to achieve this we expand the corresponding source functions of Eqs. (5) and (11) in terms of the channel wave functions

$$|\,[Y_p\Phi_h]_{j_t m_t}\rangle = \sum_{m_p m_h} (j_p\, m_p\; j_h\, m_h \,|\, j_t\, m_t) \times |\, Y_{j_p m_p}\Phi_{j_h m_h}\rangle, \tag{A1}$$

where $Y_{j_p m_p}$ is the spin-angle wave function of particle p, and $\Phi_{j_h m_h}$ is the hole wave function of nucleus B. The source function can be expanded in the following way:

$$|\,\rho\rangle = \sum_{j_t m_t}\sum_{ph}^{N_c} \rho_{ph}^{(j_t m_t)}(r)\,\frac{1}{r}\,|\,[Y_p\Phi_h]_{j_t m_t}\rangle\,. \tag{A2}$$

In (A2) N_c denotes the total number of allowed particle-hole states. The radial source function is then given by inversion of Eq. (A2)

$$\rho_{ph}^{(j_t m_t)}(r) = r\,([Y_p\Phi_h]_{j_t m_t}\,|\,\rho\rangle\,. \tag{A3}$$

After some lengthy angular momentum algebra we obtain the following result for photon scattering, Eq. (11):

$$\begin{aligned}\rho_{ph}^{(j_t m_t)}(r) &= r\,([Y_p\Phi_h]_{j_t m_t}|\rho_\gamma\rangle \\ &= (-4i)\,\frac{f_{\gamma N\Delta}}{M_\Delta}\, i^{l_h - l_p}\,\hat{j}_t\,\hat{j}_p\,\hat{j}_h\,\hat{l}_h\,(j_t\; -m_t\; j_t\, m_t \,|\, 0\,0)\;(|\vec{q}_\gamma|r)\;\phi_{n_h\,(l_h\,\frac{1}{2})\,j_h}(r)\;\varepsilon_{\vec{q}\,\lambda\,(1\,-m_t)} \\ &\quad\times\sum_{l_t,\,l'} i^{l_t}\,j_{l_t}(|\vec{q}_\gamma|r)\;\hat{l}_t^2\;(l_h\,0\;l_t\,0\,|\,l_p\,0)\;\hat{l}'\;(l_t\,0\,1\,0\,|\,l'\,0)\;W(l_t\,1\,j_t\,1\,,\,l'\,1)\;(l'\,0\,1\;-m_t\,|\,j_t\;-m_t) \\ &\quad\times\begin{Bmatrix} l_p & \frac{3}{2} & j_p \\ l_h & \frac{1}{2} & j_h \\ l_t & 1 & j_t \end{Bmatrix}.\end{aligned} \tag{A4}$$

For pion scattering, Eq. (5), we obtain

$$\begin{aligned}\rho_{ph}^{(j_t m_t)}(r) &= r\,([Y_p\Phi_h]_{j_t m_t}|\rho_\pi\rangle \\ &= (-2)\,\frac{f_{\pi N\Delta}}{M_\pi}\,i^{l_h-l_p}\,\hat{j}_t\,\hat{j}_p\,\hat{j}_h\,\hat{l}_h\,(j_t\;-m_t\;j_t\,m_t\mid 0\,0)\;(|\vec{q}_\pi|r)\,\phi_{n_h\,(l_h\,\frac{1}{2})\,j_h}(r)\,\delta_{m_t,0} \\ &\times(1\,\nu\,\frac{1}{2}\,\tau_h\mid\frac{3}{2}\,\tau_\Delta)\sum_{l_t} i^{l_t}\,j_{l_t}(|\vec{q}_\pi|r)\,\hat{l}_t^2\,(l_t\,0\,1\,0\mid j_t\,0)\,(l_h\,0\,l_t\,0\mid l_p\,0)\begin{Bmatrix} l_p & \frac{3}{2} & j_p \\ l_h & \frac{1}{2} & j_h \\ l_t & 1 & j_t \end{Bmatrix}. \end{aligned} \tag{A5}$$

In Eqs. (A4) and (A5), $\phi_{n_h\,(l_h\,\frac{1}{2})\,j_h}(r)$ denotes the radial hole wave function with quantum numbers $(n_h\;l_h\;j_h)$; $j_l(x)$ is the spherical Bessel function of the first kind and $\hat{x}=\sqrt{2x+1}$. The Clebsch-Gordan coefficient $(1\,\nu\;\frac{1}{2}\,\tau_h\mid\frac{3}{2}\,\tau_h+\nu)$ describes the isospin coupling coefficient of the pion scattering process. The isospin projections $\nu=-1,0,+1$ correspond to π^-,π^0,π^+ scattering, respectively; $\tau_h=\pm\frac{1}{2}$ is the projection of the proton and neutron hole state, respectively.

APPENDIX B: EXPLICIT FORMULAS FOR COHERENT PION PRODUCTION

Here we derive the formulas for the coherent pion production, i.e., the emission of a pion with the residual nucleus in its ground state. The transition amplitude is obtained by acting with the $\pi N\Delta$-deexcitation operator $F_{\pi N\Delta}(\vec{q}_\pi')$ onto the wave function $|\psi\rangle$ of the $(B+\Delta)$ system. First, we expand the wave function $|\psi\rangle$ into multipoles

$$|\psi\rangle = \sum_{j_t m_t}\sum_{ph}^{N_c}\psi_{ph}^{(j_t m_t)}(r)\,\frac{1}{r}\,|[Y_p\Phi_h]_{j_t m_t}\rangle, \tag{B1}$$

where

$$\psi_{ph}^{(j_t m_t)}(r) = r\,([Y_p\Phi_h]_{j_t m_t}\mid\psi\rangle\,. \tag{B2}$$

Here the wave function $|\psi\rangle$ is calculated starting from Eq. (A4) for coherent pion photoproduction and starting from Eq. (A5) for elastic pion scattering. With the help of the radial wave function $\psi_{ph}^{(j_t m_t)}(r)$ we can rewrite the transition amplitudes for elastic pion scattering and coherent pion photoproduction as

$$\begin{aligned}T = \langle\Phi_A|F_{\pi N\Delta}(\vec{q}_\pi')|\psi\rangle &= \sum_{j_t m_t}\sum_{ph}^{N_c}\left(2\sqrt{4\pi}\right)\frac{f_{\pi N\Delta}}{M_\pi}\,i^{l_h-l_p}\,\frac{\hat{j}_p\,\hat{j}_h}{\hat{j}_t}\,\hat{l}_h\;|\vec{q}_\pi'|\,Y_{j_t}^{m_t}(\hat{q}_\pi') \\ &\times\sum_{l_\pi}(-i)^{l_\pi}\,\hat{l}_\pi^2\,(l_\pi\,0\,1\,0\mid j_t\,0)\,(l_h\,0\,l_\pi\,0\mid l_p\,0)\begin{Bmatrix} l_p & \frac{3}{2} & j_p \\ l_h & \frac{1}{2} & j_h \\ l_\pi & 1 & j_t \end{Bmatrix} \\ &\times(1\,\nu\;\tfrac{1}{2}\,\tau_h\mid\tfrac{3}{2}\,\tau_\Delta)\int dr\,r\,j_{l_\pi}(|\vec{q}_\pi'|r)\,\psi_{ph}^{(j_t m_t)}(r)\,\phi_{n_h\,(l_h\,\frac{1}{2})\,j_h}(r)\,. \end{aligned} \tag{B3}$$

APPENDIX C: EXPLICIT FORMULA FOR ELASTIC COMPTON SCATTERING

In this appendix we show the explicit formula for the elastic Compton scattering, i.e., the residual nucleus is in its ground state. Using the same expansion as in Appendix B for the radial wave function $\psi_{ph}^{(j_t m_t)}(r)$ we obtain the following for the resonant transition amplitude:

$$\begin{aligned}T_\Delta^\gamma = \langle\Phi_A|F_{\gamma N\Delta}(\vec{q}_\gamma')|\psi\rangle &= \sum_{j_t m_t}\sum_{ph}^{N_c}(4i)\,\frac{f_{\gamma N\Delta}}{M_\Delta}\,i^{l_h-l_p}\,\hat{j}_p\,\hat{j}_h\,\hat{l}_h\;|\vec{q}_\gamma'|\,d^{j_t}_{-\lambda' m_t}(\hat{q}_\gamma') \\ &\times\sum_{l_t,l'}(-i)^{l_t}\,\hat{l}_t^2\,\hat{l}'\,W(l_t\,1\,j_t\,1\,,\,l'\,1)\,(l_t\,0\,1\,0\mid l'\,0)\,(l'\,0\,1\;-\lambda'\mid j_t-\lambda') \\ &\times(l_h\,0\,l_t\,0\mid l_p\,0)\int dr\,r\,j_{l_t}(|\vec{q}_\gamma'|r)\,\psi_{ph}^{(j_t m_t)}(r)\,\phi_{n_h\,(l_h\,\frac{1}{2})\,j_h}(r)\begin{Bmatrix} l_p & \frac{3}{2} & j_p \\ l_h & \frac{1}{2} & j_h \\ l_t & 1 & j_t \end{Bmatrix}. \end{aligned} \tag{C1}$$

[1] For reviews on the experimental and theoretical situation of Δ's in nuclei, see for example: J. Hüfner, Phys. Rep. **21**, 1 (1975); G. E. Brown and W. Weise, *ibid.* **22**, 279 (1975); E. J. Moniz, in *Nuclear Physics with Heavy Ions and Mesons*, edited by A. Balian, M. Rho, and G. Ripka (North-Holland, Amsterdam, 1978), Vol. 2, p. 433; J. M. Eisenberg and D. S. Koltun, *Theory of Meson Interactions with Nuclei* (Wiley, New York, 1980).
[2] T. E. O. Ericson and W. Weise, *Pions in Nuclei* (Oxford University Press, Oxford, England, 1988).
[3] J. Ahrens, Nucl. Phys. **A446**, 229c (1985).
[4] J. Arends, J. Eyink, A. Hegerath, K. G. Hilger, B. Mecking, G. Nöldeke, and H. Rost, Phys. Lett. **98B**, 423 (1981).
[5] J. Arends, N. Floss, A. Hegerath, B. Mecking, G. Nöldeke, and R. Stenz, Z. Phys. A **311**, 367 (1983).
[6] H. Rost, Ph.D. thesis, University of Bonn, 1980.
[7] P. Carlos *et al.*, Nucl. Phys. **A431**, 573 (1984).
[8] A. S. Carroll *et al.*, Phys. Rev. C **14**, 635 (1974).
[9] F. Binon *et al.*, Nucl. Phys. **B17** 168 (1970).
[10] L. S. Kisslinger and W. L. Wong, Ann. Phys. **99**, 374 (1976).
[11] M. Hirata, J. H. Koch, F. Lenz, and E. J. Moniz, Phys. Lett. **70B** 281 (1977); Annu. Phys. **120**, 205 (1979).
[12] Y. Horikawa, M. Thies, and F. Lenz, Nucl. Phys. **A345**, 386 (1980).
[13] J. H. Koch, E. J. Moniz, and N. Ohtsuka, Ann. Phys. **154**, 99 (1984).
[14] J. H. Koch and N. Ohtsuka, Nucl. Phys. **A435**, 765 (1985).
[15] C. Gaarde, Annu. Rev. Nucl. Sci. **41**, 187 (1991).
[16] J. Delorme and P. A. M. Guichon, in Proceedings of the 10th Biennale de Physique Nucleaire, Aussois, 1989, (unpublished), p. C.4.1.
[17] F. Osterfeld, Rev. Mod. Phys. **64**, 491 (1992).
[18] D. Contardo *et al.*, Phys. Lett. B **168**, 331 (1986).
[19] V. G. Ableev *et al.*, Sov. Phys. JETP Lett. **40**, 763 (1984) .
[20] D. A. Lind, Can. J. Phys. **65**, 637 (1987).
[21] B. E. Bonner *et al.*, Phys. Rev. C **18**, 1418 (1978).
[22] T. Udagawa, S. W. Hong, and F. Osterfeld, Phys. Lett. B **245**, 1 (1990).
[23] J. Delorme and P. A. M. Guichon, Phys. Lett. B **263**, 157 (1991).
[24] M. Ericson, Nucl. Phys. **A518**, 116 (1990).
[25] V. F. Dmitriev and T. Suzuki, Nucl. Phys. **A438**, 697 (1985).
[26] G. Chanfray and M. Ericson, Phys. Lett. B **141**, 163 (1984).
[27] T. Hennino *et al.*, Phys. Lett. B **283**, 42 (1992).
[28] T. Hennino *et al.*, Phys. Lett. B **303**, 236 (1993).
[29] P. Oltmanns, F. Osterfeld, and T. Udagawa, Phys. Lett. **B299**, 194 (1993).
[30] F. Osterfeld, B. Körfgen, P. Oltmanns, and T. Udagawa, Phys. Scr. **48**, 95 (1993).
[31] E. Oset, P. F. de Cordoba, J. Nieves, and M. J. Vicente-Vacas, Phys. Scr. **47**, 793 (1993).
[32] T. E. O. Ericson, Nucl. Phys. **A560** 458 (1993).
[33] T. Udagawa, P. Oltmanns, F. Osterfeld, and S. W. Hong, Phys. Rev. C **49**, 3162 (1994).
[34] E. Oset, H. Toki, and W. Weise, Phys. Rep. **83**, 281 (1982).
[35] I. Laktineh, W. M. Alberico, J. Delorme, and M. Ericson, Nucl. Phys. **A555**, 237 (1993).
[36] M. B. Johnson, in *Pion-Nucleus Physics: Future Directions and New Facilities at LAMPF*, Proceedings of the Los Alamos Conference on Pion-Nucleus Physics, edited by R. J. Peterson and D. D. Strottman, AIP Conf. Proc. No. 163 (AIP, New York, 1988), p. 352.
[37] M. B. Johnson and D. J. Ernst, Ann. Phys. **219**, 266 (1992).
[38] J. H. Koch and E. J. Moniz, Phys. Rev. C **27**, 751 (1983).
[39] N. M. Kroll and M. A. Ruderman, Phys. Rev. **93**, 233 (1954).
[40] H. Pilkuhn, *Relativistic Particle Physics* (North-Holland, Amsterdam, 1967).
[41] M. Schmitz, Annual Report 1992/93, Institut für Kernphysik, University of Mainz.
[42] F. Wissmann, Ph.D. thesis, University of Mainz, 1993.